Materials Today Bio 16 (2022) 100417

Contents lists available at ScienceDirect

Materials Today Bio

journal homepage: www.journals.elsevier.com/materials-today-bio

Polymeric nanoparticles targeting Sialyl-Tn in gastric cancer: A live tracking under flow conditions

Francisca Diniz [a,b,c], Maria Azevedo [a], Flávia Sousa [a,d,e,1], Hugo Osório [a,b], Diana Campos [a,b,2], Paula Sampaio [a], Joana Gomes [a,b], Bruno Sarmento [a,d,e], Celso A. Reis [a,b,c,f,*]

[a] i3S - Instituto de Investigação e Inovação em Saúde, Universidade do Porto, 4200-135 Porto, Portugal
[b] IPATIMUP -Institute of Molecular Pathology and Immunology, University of Porto, 4200-135 Porto, Portugal
[c] ICBAS- Instituto de Ciências Biomédicas Abel Salazar, Universidade do Porto, 4050-313 Porto, Portugal
[d] INEB- Instituto Nacional de Engenharia Biomédica, Universidade do Porto, 4200-135 Porto, Portugal
[e] CESPU-IUCS, 4585-116 Gandra, Portugal
[f] FMUP- Faculty of Medicine, University of Porto, 4200-319 Porto, Portugal

ARTICLE INFO

Keywords:
Polymeric nanoparticles
Gastric cancer
Sialyl-Tn antigen
Microfluidics

ABSTRACT

Drug delivery using nanoparticles (NPs) represents a potential approach for therapy in cancer, such gastric cancer (GC) due to their targeting ability and controlled release properties. The use of advanced nanosystems that deliver anti-cancer drugs specifically to tumor cells may strongly rely on the expression of cancer-associated targets. Glycans aberrantly expressed by cancer cells are attractive targets for such delivery strategy. Sialylated glycans, such as Sialyl-Tn (STn) are aberrantly expressed in several epithelial tumors, including GC, being a potential target for a delivery nanosystem. The aim of this study was the development of NPs surface-functionalized with a specific antibody targeting the STn glycan and further evaluate this nanosystem effectiveness regarding its specificity and recognition capacity. Our results showed that the NPs surface-functionalized with anti-STn antibody efficiently are recognized by cells displaying the cancer-associated STn antigen under static and live cell monitoring flow conditions. This uncovers the potential use of such NPs for drug delivery in cancer. However, flow exposure was disclosed as an important biomechanical parameter to be taken into consideration. Here we presented an innovative and successful methodology to live track the NPs targeting STn antigen under shear stress, simulating the physiological flow. We demonstrate that unspecific binding of NPs agglomerates did not occur under flow conditions, in contrast with static assays. This robust approach can be applied for *in vitro* drug studies, giving valuable insights for *in vivo* studies.

1. Introduction

Gastric cancer (GC) represents the fifth most incident and the third most lethal cancer worldwide with an incidence of 1 million new cases per year [1]. This high mortality of GC is associated with a late diagnosis, as the patient becomes symptomatic in an advanced stage, limiting the therapeutic options and the efficacy of treatment [2]. Recent approaches applying nanotherapeutics are recognized as potential strategies to improve patient treatment [3]. The use of nanoparticles (NPs) that are capable of remaining in the blood circulation for an extended time period and that can be engineered to target cancer cells represent a major opportunity to increase therapy efficacy. NPs need to avoid nonspecific interactions with healthy cells and circumvent *in vivo* barriers to avoid side effects and loss of drug-carrying NPs. The control of the NPs surface constituents is crucial for the determination of their *in vivo* interaction and optimization of the nano-drug delivery efficiency [4–6]. Moreover, targeting cancer cells with functionalized NPs carrying anti-cancer drugs allows an efficient therapy reducing the major side effects commonly caused by drugs used in oncology [3,4,7].

Poly (lactic-*co*-glycolic acid) (PLGA) is a widely used polymer for production of NPs due to its biocompatibility and biodegradability, long-standing track record in biomedical applications and well-documented utility for sustained drug release [8,9]. For that it was approved by US Food and Drug Administration (FDA) and European Medicines Agency

* Corresponding author. i3S - Instituto de Investigação e Inovação em Saúde, Universidade do Porto, 4200-135 Porto, Portugal.
E-mail address: celsor@ipatimup.pt (C.A. Reis).
[1] Flávia Sousa -Instituto Italiano di Tecnologia, ITT: via Morego 30, Génova.
[2] Diana Campos - Max-Planck-Institut fuer Herz-und Lungenforschung, Ludwigstrasse 43, Bad Nauheim, 61231, Germany.

https://doi.org/10.1016/j.mtbio.2022.100417
Received 26 May 2022; Received in revised form 29 August 2022; Accepted 1 September 2022
Available online 3 September 2022

(EMA) for medical applications [10]. The surface modification of PLGA-NPs plays an important role with respect to targeting strategy. When combined with polyethylene glycol (PEG) they increased the hydrophilicity of the formulation resulting in a robust particle with enhanced blood circulation time, avoiding its immunogenicity and improving the pharmacokinetics properties of drugs by escaping opsonization [8,11].

Despite the advances of nanotherapeutics in medicine, there is still major limitations regarding cancer cell targeting and drug delivery. To improve the specificity of the NPs, defined antibodies targeting ligands such as carbohydrates antigens aberrantly expressed by cancer cells might be attached to the surface of NPs by functionalization [12]. The aberrant biosynthesis of glycans are common features in cancer leading to the display of specific cancer-associated glycan structures with important roles in tumor progression and metastization [13–15]. Moreover, the use of glycans as targets for cell delivery has been shown to be an effective strategy for cell-selective drug delivery [7]. NPs functionalized with antibodies or molecules targeting carbohydrates would provide a largely multi-valent technique of interactions with target cells showing increased local ligands level on design surfaces [4,7,12].

Sialyl-Tn (STn), a truncated O-glycan containing sialic acid residue, is aberrantly expressed in several epithelial cancers, including GC [15–18]. This antigen is not expressed in normal tissues, whereas it is highly expressed in carcinomas and associated with aggressive tumors such as those with chemotherapy resistance and poor prognosis [18–20]. The biosynthesis of the STn antigen is dependent on the expression of the sialyltransferase ST6GalNAc1 [18,21], as well as to the mutations of the gene encoding the molecular chaperone COSMC [22,23]. We previously showed that STn plays a critical role during cancer progression impairing clinical outcome and leading to poor prognosis and a more aggressive phenotype in GC patients [18,24]. STn-monoclonal antibodies coated on europium NPs were previously used for diagnostic purposes in cancer [25]. Given its expression and association with GC malignant features, the STn antigen has a higher potential as a target for a new NP system using an antibody directed to STn.

The study of NP-target cell interactions under flow conditions is crucial to evaluate the cellular responses in physiological-like environments. In terms of NPs applicability, flow stimulation can critically affect the efficacy of the targeting or the drug delivery accumulation in the tumor region [26,27]. Thus, the physiological flow stimulation is important to mimic the *in vivo* conditions for NPs risk management. Contrarily to under flow conditions, static culture promotes the sedimentation of NPs, supporting the local increase in the NPs concentration, and resulting in unspecific binding to the target cells [28–30]. In addition, it has been reported that flow can affect cell-NP interactions and therefore the NP uptake via the cells. Accordingly, rates of NPs exocytosis and endocytosis by cells have been observed with slight differences upon perfusion [27,31,32]. Thus, the cell's response under flow should be considered for improved validation of the targeting.

Here, we developed a nanodelivery system functionalized with an antibody against STn and we further evaluate their interaction with cells and ability to target the tumor glycan in both static and under flow conditions. For this purpose, we applied a perfusion system in a controlled microenvironment to better understand the interaction of the developed targeted polymeric NPs with glycoengineered cells expressing STn antigen, under a flow-induced shear stress. This new tool to study the effect of the NP interaction with cells under live flow conditions, provide the opportunity to track the NPs for a time period and analyze their interaction with the target cell.

2. Material and methods

2.1. Synthesis of PLGA-PEG-COOH nanoparticles

The Lapatinib-loaded PLGA-PEG-COOH NPs were prepared by using nanoprecipitation method [33,34]. PLGA-PEG-COOH block copolymer was used to present the carboxylic acid on the NP surface, allowing the carbodiimide reaction to amine group from the antibody. Briefly, 19 mg of Poly(lactide-*co*-glycolide) (PLGA) 5004A (provided by Corbion) and 1 mg of Poly(lactide-*co*-glycolide)-*b*-poly(ethylene glycol)-carboxylic acid endcap (PLGA-PEG-COOH) (PolySCiTech) were added to 1 mg of Lapatinib (Sigma-Aldrich, Ref. CDS022971) (dissolved in DMSO, 20 μl) and left in 1,980 mL of acetone (ThermoFisher) to allow the complete dissolution. Further, this organic solution was transferred using a 25G needle to an aqueous solution of 0,5% (w/v) Pluronic F-127 (Sigma-Aldrich) (20 mL) under magnetic stirring (300 rpm) for 3h and the remaining organic solvent was removed by evaporation. Finally, NPs were washed with MiliQ water, using 100 kDa Amicon® filters, centrifuged for 20min at 2,000g, thrice. The NPs were resuspended in 1,5 mL of PBS in the final. The same nanoprecipitation method was also used to produce Lapatinib-loaded PLGA and empty NPs without the presence of PLGA-PEG-COOH and Lapatinib. Fluorescent NPs were produced to allow NP tracking under flow assays, following the same nanoprecipitation method described in a previous study [32]. Briefly, it was added 2 mg of Poly(lactide-*co*-glycolide)-Fluorescein (PolySCiTech), that corresponds to 5% of PLGA-FITC of the theoretical mass. As the FITC conjugation is covalent, early release of the fluorophore from NPs is not expected.

2.2. Nanoparticle-antibody conjugation

Monoclonal antibody (mAb) B72.3 (anti-STn) [35] was purified from hybridoma culture media using the HiTrapTM Protein G HP 1 mL columns of purification (Sigma-Aldrich) The conjugation of NPs with anti-STn (B72.3) or IgG1 Isotype Control Purified Mouse Monoclonal IgG antibody (R&D Systems) was performed via carbodiimide chemistry which allowed to chemically link the antibody ligand to the COOH group of PLGA-PEG present on the surface of NPs. NPs (150 μL, 1:10 of the final NP concentration 14 mg/mL) were resuspended in 820 μL of 2-(N-morpholino) ethanesulfonic acid (MES) buffer (0.1 M, pH 5.5). Then, were incubated with 27 μL of 1-ethyl-3(3-dimethylaminopropyl) carbodiimide (EDC) (22 mg/mL) and 3 μL of N-hydroxysuccinimide (NHS) (8 mg/mL) for 30 min at room temperature (RT), protected from light and with gentle stirring. NPs were washed twice with PBS (centrifuged at 5000g for 8min, RT), the last resuspension was performed in 500 μL of PBS. The resulting activated NPs were reacted with 33 μg of B72.3 or IgG1 antibody, resuspended in 500 μL of PBS, for 2h at room temperature and gentle stirring. Further, the functionalized NPs were washed twice using PBS and kept at 4 °C in 1 mL PBS until use. These last two washes were kept to be quantified further in conjugation efficiency evaluation by indirect method.

2.3. Physicochemical characterization of the formulations

After washing, all the formulations were physiochemically characterized regarding the particle size (nm), polydispersity index and surface charge (ζ-potential in mV) using Malvern Zetasizer Nano ZS instrument (Malvern Instruments Ltd). The NPs before measuring were diluted in sodium chloride (NaCl) 10 mM, pH 7.4.

2.4. Morphology of nanoparticles

The morphology of the NPs was observed though Transmission Electron Microscopy (TEM). Briefly, 10 μL of each NPs sample were mounted on nickel grids and left to stain for 2 min approximately. Afterwards, the excess liquid was removed with filter paper, and a Uranyl Acetate solution (1%) was added and left to incubate for 10s. Samples were viewed on a JEOL JEM 1400 TEM (JEOL, Tokyo, Japan) operated at 80 kV, and images were digitally recorded using a CCD digital camera Orius 1100W (Tokyo, Japan).

2.5. Association efficacy, drug loading and conjugation efficiency

2.5.1. LC-MS

The association efficacy and drug loading of Lapatinib loaded in NPs was determined by LC-MS. NPs formulations were exposed overnight at freeze dryer and then were resuspend in dimethylformamide for drug extraction. The LC-MS analysis was done in an Ultimate 3000 liquid chromatography system coupled to a Q-Exactive Hybrid Quadrupole-Orbitrap mass spectrometer (Thermo Scientific, Bremen, Germany). Samples were loaded onto a trapping cartridge (Acclaim PepMap C18 100 Å, 5 mm × 300 μm i. d., 160454, Thermo Scientific, Bremen, Germany) in a mobile phase of 2% AcCN, 0.1% FA at 30 μL/min. After 1 min loading, the trap column was switched in-line to a EASY-Spray nano Flow Emitter with 10 μm inner diameter without transfer line (ES993, Thermo Scientific, Bremen, Germany) at 1 μL/min. Separation was achieved by mixing A: 0.1% FA and B: 80% AcCN, 0.1% FA with the following gradient: 1 min (2.5% B to 99% B), 3 min (hold 99% B). Subsequently, the system was equilibrated with 2.5% B. Data acquisition was controlled by Xcalibur 4.0 and Tune 2.9 software (Thermo Scientific, Bremen, Germany). The mass spectrometer was operated in the data-dependent (dd) positive acquisition mode alternating between a full scan (m/z 380–1300) and subsequent HCD MS/MS of the 5 most intense peaks from a full scan (normalized collision energy of 27%). The ESI spray voltage was 1.9 kV. The global settings were as follows: use lock masses best (m/z 445.12003), lock mass injection Full MS and chrom. peak width (FWHM) of 15 s. The full scan settings were as follows: 70 k resolution (m/z 200), AGC target 3×10^6, maximum injection time 120 ms; dd settings: minimum AGC target 8×10^3, intensity threshold 7.3×10^4, charge exclusion: unassigned, 1, 8, >8, peptide match preferred, exclude isotopes on, and dynamic exclusion 5 s. The MS2 settings were as follows: microscans 1, resolution 35 k (m/z 200), AGC target 2×10^5, maximum injection time 110 ms, isolation window 4.0 m/z, isolation offset 0.0 m/z, dynamic first mass, and spectrum data type profile.

Association Efficacy (%) = (Mass of the drug in NPs / Initial Mass of drug in the NPs) x 100

Drug loading capacity (%) = (Mass of the drug in NPs / Initial Mass of the NPs) x 100

We also performed LC-MS to confirm the conjugation efficiency of B72.3 or IgG antibody to NPs, conjugated with Lapatinib, by direct method. Proteomic sample preparation and data acquisition was performed as previously described [36]. Data analysis was carried out with the software Proteome Discoverer version 2.5.0.400 (Thermo Scientific). Protein identification analysis was conducted by the Sequest node using the SwissProt Protein database (2020_05, 565,553 entries). Protein Label Free Quantitation was performed by the Minora and Precursor Ions Quantifier nodes.

Conjugation Efficiency (%) = (Mass of antibody in NPs / Initial Mass of antibody in the NPs) x 100

2.5.2. Enzyme-linked immunosorbent assay (ELISA)

The binding efficiency of B72.3 antibody and IgG1 control to NPs was also quantified by indirect method using enzyme-linked immunosorbent assay (ELISA). ELISA was performed using 96-well MaxiSorp plates (Nunc, Denmark). Plates were coated overnight at 4 °C with 10 μL of supernatant of each sample of NPs or the positive control sample (same amount of antibody used in the functionalization process) in bicarbonate-carbonate buffer (pH 9.6) and blocked in PLI-P (PO4, Na/K, 1% Triton X-100 (Sigma-Aldrich), 1% BSA) buffer (pH 7.4) for 1 h at RT. Following washing, plates were incubated with Goat anti-mouse HRP antibody (1:5000) (Jackson ImmunoResearch) for 1h at RT. Plates were developed with TMB + substrate (Thermo Scientific), reactions were stopped with 0.5 M H_2SO_4 (VWR), and absorbance was read at 450 nm using SynergyMx™ Multimode Microplate Reader (BioTek™, USA). All samples were done in triplicate. The obtained absorbance values were used to calculate the conjugation efficiency (%).

Conjugation Efficiency (%) = ((Absorbance of the input – Absorbance of the sample) / Absorbance of the input) x 100

2.6. ImmunoTEM

The antibody bound to NP was visually confirmed by ImmunoTEM. Briefly, approximately 10 μL of NPs were mounted on nickel grids and left to stain for 20min. Then 1% BSA, PBS was added for 30min at room temperature to block any unspecific signal. Afterwards, gold goat anti-mouse (1:50) (Abcam) was added for 20min. Followed by 6 washes with PBS and 6 washes with distilled water, 3min each. Finally, 5 μL of Uranyl Acetate solution (1%) was added and left to incubate for 10s. Samples were viewed on a JEOL JEM 1400 transmission electron microscope (JEOL, Tokyo, Japan) operated at 80 kV, and images were digitally recorded using a CCD digital camera Orius 1100W (Tokyo, Japan).

2.7. Cell lines and cell culture reagents

Gastric carcinoma cell line MKN45 (MKN45 WT) and AGS (AGS WT) were obtained from the Japanese Cancer Research Bank (Tsukuba, Japan) and the American Type Culture Collection (Manassas, VA, USA), respectively. The MKN45 SimpleCell (MKN45 SC) and AGS SimpleCell (AGS SC) models were generated by targeting the C1GALT1 (COSMC) gene using zinc-finger nuclease precise gene editing, which results in knockout COSMC, as previously described [37]. Cells were grown in monolayer culture in cell culture flasks, maintained at 37 °C in an atmosphere of 5% CO_2, in RPMI 1640 GlutaMAX medium (Gibco, Thermo Fisher Scientific, Waltham, MA, USA), supplemented with 10% fetal bovine serum (FBS) (Biowest, Riverside, MO, USA).

2.8. Cell-nanoparticle interaction studies under static conditions

2.8.1. Flow cytometry

MKN45 WT and MKN45 SC cells were seeded in 6-well plates 48h before analysis. Cells were detached using Versene solution (ThermoFisher), and 1million cells were used in each condition. Cells suspension was fixed with 2% Paraformaldehyde (PFA) (Alfa Aesar), PBS for 20min at RT, and then washed twice with PBS at 350g for 5min. Cells were permeabilizated with 0,1% Triton, PBS for 5min at 4 °C and washed twice with PBS. Afterwards, cells were incubated under gentle agitation at RT with functionalized NPs (100 μg/mL), B72.3 antibody (33 μg) or IgG1 antibody (33 μg) for 2h. After, cells were washed and incubated with the secondary antibody goat anti-mouse Alexa Fluor® 488 (1:200) (Invitrogen) for 30min in the dark. Cells were washed and resuspended in PBS, strained and labelled with DAPI (2 μg/mL) (Sigma-Aldrich). The same method was used for samples previously treated with the neuraminidase enzyme (0,2U/ml) (Sigma-Aldrich) diluted in simple medium during 1h30min at 37 °C. Cells were incubated with B72.3 functionalized PLGA-PEG NPs (100 μg/mL) and monoclonal antibody to the Tn antigen (5F4)) (undiluted) [38]. Cells suspension was analyzed using BD FACS Canto™ II (BD Biosciences, San Jose, CA, USA). Three independent experiments were conducted. Data were analyzed using FlowJo (BD Biosciences, San Jose, CA, USA).

2.8.2. Immunofluorescence

A defined concentration of 4×10^4 cells/mL of MKN45 WT and MKN45 SC were seeded in a 12-well standard microscope glass slide with a removable silicone chamber (Ibidi GmbH, Munich, Germany) and left

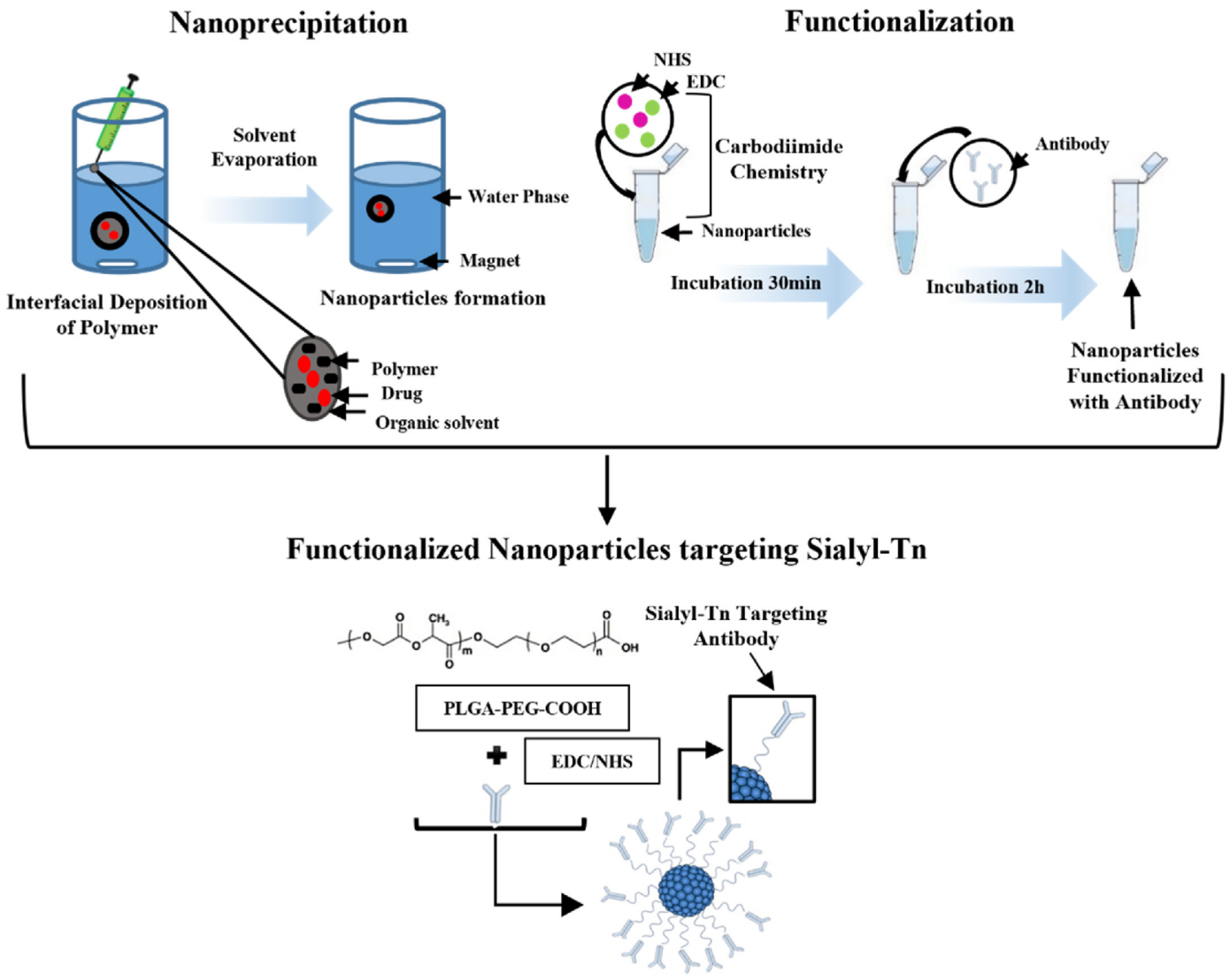

Scheme 1. Schematic representation of methodology behind the development of encapsulated and functionalized nanoparticles.

in the incubator for 48h. Cells were exposed during different time points (0h, 2h, 4h and 6h) to both functionalized NPs independently. After that were washed twice with PBS and fixed with 4% PFA for 15min followed by permeabilization with 0,1% Triton X-100-PBS for 5min at 4 °C. Blocking was done with Goat serum (1:5) (Dako) in 10% BSA-PBS at room temperature for 30min. Goat anti-mouse Alexa Fluor® 488 secondary antibody (1:200) (Invitrogen) and Alexa Fluor 568 Phalloidin (1:40) (ThermoFisher) were diluted in 5% BSA, PBS and PBS, respectively, and cells were incubated for 30min. Nuclear stain was done with DAPI (1:100) in PBS for 10min and the preparation was mounted using Vectashield. Imaging was performed on a Zeiss AxioImager Z1(Carl Zeiss, Oberkochen, Germany) equipped with a Axiocam MR ver3.0 (Carl Zeiss, Germany), and an HXP 120 light source (metal-halide lamp) using a Plan-Apochromat 20x/0.8 or a Plan-Apochromat 40x/1.30 Oil objective. For DAPI, Alexa Fluor 488 and Alexa Fluor 568 phalloidin acquisition, the following filter cube sets were used, respectively: Excitation: G 365 Beam Splitter: FT 395 Emission: BP 445/50; Excitation: BP 470/40 Beam Splitter: FT 495 Emission: BP 525/50 and Excitation: BP 450–490 Beam Splitter: FT 510 Emission: BP 515–565.

2.8.3. Metabolic activity assay

Metabolic activity was measured using a resazurin reduction assay. Cells were seeded in triplicate in a 96-well plate at a density of 1×10^4 cells/well and treated with 100 μg/mL of functionalized and non-functionalized NPs. Cells treated with hydrogen peroxide (H_2O_2) and untreated cells were used as positive and negative controls, respectively. After 5,5h and 24h, 0.02 mg/ml resazurin (Sigma-Aldrich) was added to the cells and incubated for additional 2h at 37 °C. Fluorescence intensity (ex. 530 nm; em. 590 nm) was measured using a Synergy™ Mx microplate reader (Agilent, Santa Clara, CA, USA).

The same experimental protocol was used to measure the metabolic activity of the cells after 24h and 48h of treatment with 1 μg/mL of free Lapatinib, IgG Functionalized Lapatinib-loaded PLGA-PEG NPs (NLIgG) and B72.3 Functionalized Lapatinib-loaded PLGA-PEG NP (NLB72.3).

2.9. Cell-nanoparticle interaction studies under flow conditions

The experiments under flow were performed using a peristaltic pump system (ISMATEC, model ISM931C). Initially, 7×10^5 cells/channel were seeded in a 6-channel polymer μ-slide suitable for flow assays (μ-Slide VI 0.4, Ibidi GmbH, Munich, Germany), previously coated with N- Poly-L-Lysine (PLL) (Sigma-Aldrich) (10 μg/mL). Cells were grown for 72h, until a confluent cellular monolayer was formed. Afterwards, the medium was replaced to phenol-red-reduced RPMI 1640 medium (Gibco) supplemented with 10% FBS, 25 mM HEPES buffer (Gibco) solution, 2 mM GlutaMAX (Gibco), 1% Sodium Pyruvate (Cytiva) and 1%

Table 1
Properties of functionalized and non-functionalized nanoparticles, including the mean size, polydispersity index (PdI), surface charge and conjugation efficacy (CE). The values are represented as mean values ± SD (N = 3). Non applicable (n.a.).

Nanoparticle Sample	Size (nm)	PdI	Surface Charge (mV)	CE (%) ELISA
PLGA NP (NP)	152.8 ± 2.3	0.087 ± 0.018	−12.7 ± 0.8	n.a.
PLGA-PEG-COOH NP (NPP)	147.1 ± 0.6	0.055 ± 0.009	−15.8 ± 1.2	n.a.
B72.3 Functionalized PLGA-PEG NP (NB72.3)	179.4 ± 2.5	0.174 ± 0.024	−16.0 ± 1.3	85.3 ± 0.3
IgG Functionalized PLGA-PEGNP (NIgG)	178.8 ± 2.2	0.161 ± 0.028	−14.9 ± 1.9	75.9 ± 0.4
B72.3 Adsorbed PLGA-PEG NP (NAdsB72.3)	186.7 ± 1.5	0.139 ± 0.024	−18.3 ± 0.1	64.1 ± 7.5
FITC-labelled NP (NF)	140.7 ± 1.5	0.117 ± 0.019	−12.4 ± 0.2	n.a.
B72.3 Functionalized PLGA-FITC-PEG NP (NF–B72.3)	214.5 ± 6.4	0.189 ± 0.037	−12.4 ± 1.5	88.5 ± 3.3
IgG Functionalized PLGA-FITC-PEG NP (NF-IgG)	217.6 ± 8.2	0.191 ± 0.046	−12.6 ± 1.2	80.1 ± 5.9

Penicillin-Streptomycin (100x) (Gibco). Therefore, 100 μg/mL of respective NPs were diluted in 6,5 mL of cell culture medium. Each channel of the μ-slide was connected to the tubes and to the reservoir containing the medium. Cell binding studies under flow conditions were performed live at a shear stress of 2 dyn/cm^2, for 6h. During the optimization process, we also tested 10 dyn/cm^2 and 5 dyn/cm^2, however we selected 2 dyn/cm^2, since this represented the best option for the viability of our cells and was in accordance with what was previously described in the literature (venous system associated to a shear stress between 1 and 6 dyn/cm^2). Images were acquired every 15min, using an inverted motorized Leica DMI6000 (Leica Microsystems) widefield microscope, equipped with a Hamamatsu Orca-FLASH 4.0 sCMOS camera (C11440, Hamamatsu), an HCX PL FL L 40x/0.60 CORR Ph2 objective, a Leica EL6000 light source (metal-halide lamp), and controlled through the LAS X software (version 3.5.5.19976). Samples were imaged using binning 2 × 2. Alexa Fluor 488 beads acquisition was done using the following filter cube set: Excitation: 460/40; BS: 505; Emission: 527/30. The video and image analysis were performed using ImageJ software [39].

2.10. Statistical analysis

Results are expressed as mean ± standard deviations (SD) of three independent experiments. Data were analyzed using Student's t-test for the individual group comparison, with GraphPad Prism 6.0 software (GraphPad, San Diego, CA, USA). The level of significance was set at probabilities of *p < 0.05; **p < 0.01 and ***p < 0.001.

3. Results and discussion

3.1. Production and characterization of the polymeric nanoparticles

In this study, NPs were produced by nanoprecipitation (Scheme 1), a commonly used method to encapsulate hydrophobic drugs in polymeric NPs. Then we proceeded to the functionalization of the NPs process (Scheme 1), a critical step in the success for the conjugation of the antibody to the NP based in carbodiimide chemistry method. This conjugation consists of carboxyl groups of the NPs, which must be activated by the addition of cross-linking agents, such EDC, and NHS. These two compounds, are added to improve the coupling efficiency to the group amine present on the antibody to be conjugated (IgG1 or B72.3) [40,41]. PEG was used as it has been shown to prolong NP circulating half-time which being associated with reducing nonspecific adsorption of biomacromolecules and contributing to decrease of nonspecific interactions [8].

Physical-chemical properties of NPs were assessed such as their size, surface charge and size distribution and summarized in Table 1. The size of the different formulations was ranged between 140 nm and 217 nm, with a polydispersity index (PdI) lower than 0.2, indicating a relative homogenous size distribution. All formulations presented negative surface charge, between −18 and −12 mV.

The analysis of the developed NPs by TEM showed that the surface morphology where spherical and they were well distributed (Fig. 1, A-D).

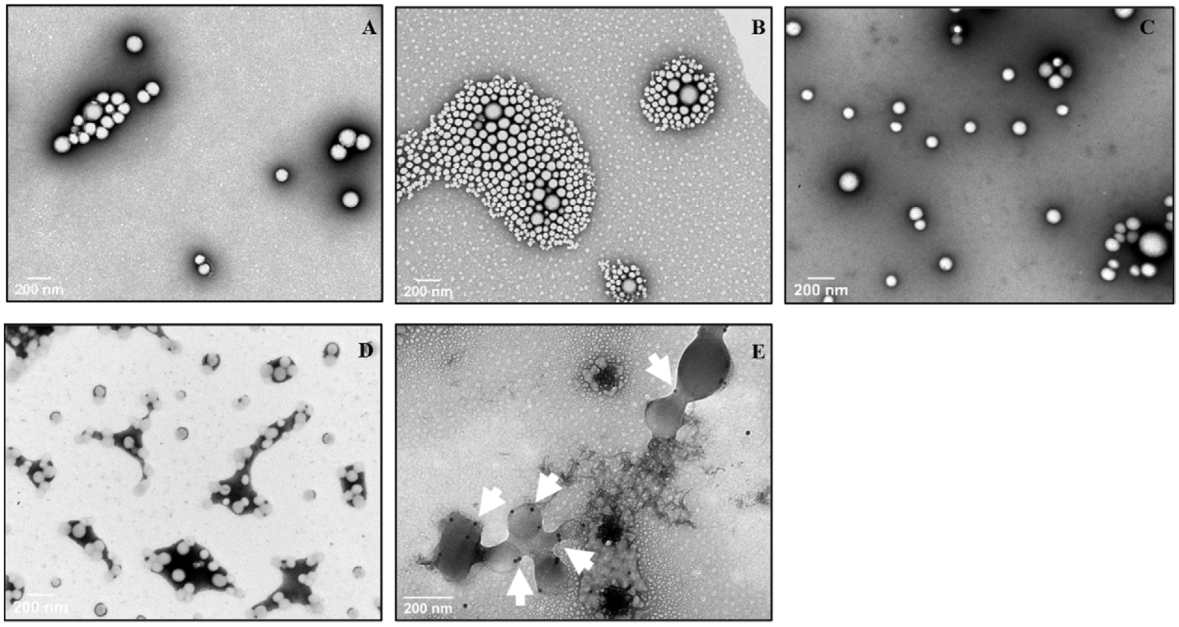

Fig. 1. Image of PLGA (A), PLGA-PEG (B), B72.3 Functionalized PLGA-PEG (C) and IgG Functionalized PLGA-PEG (D) nanoparticles obtained by Transmission Electron Microscopy (TEM). (E) Image resulting of ImunoTEM with B72.3 Functionalized PLGA-PEG nanoparticles. The white arrow represents the antibody bound to the nanoparticle. Scale bar: 200 nm.

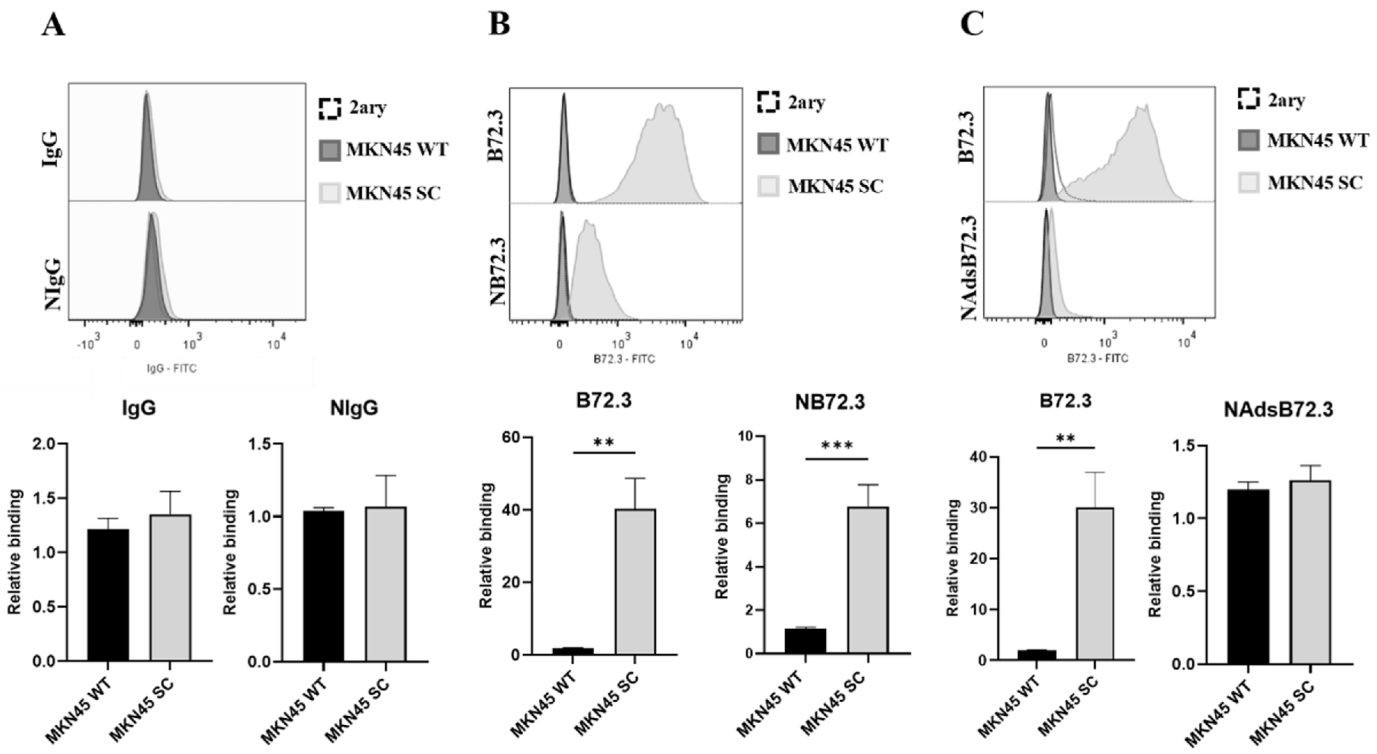

Fig. 2. Flow cytometry analysis of MKN45 WT and MKN45 SC, which were incubated with (A) IgG Functionalized PLGA-PEG NP (NIgG), (B) B72.3 Functionalized PLGA-PEG NP (NB72.3) and (C) B72.3 Adsorbed PLGA-PEG NP (NAdsB72.3) nanoparticles, to evaluate the targeting ability and specificity of the nanoparticles under static fluid conditions. Data presented as representative histograms of 3 independent experiments and mean of relative binding ± SD.

3.1.1. Conjugation efficiency of antibodies to the nanoparticles

The surface of PLGA-PEG-COOH NPs (NPP) was functionalized with one of the two antibodies: the monoclonal antibody B72.3 or a control mouse IgG. As mentioned before, B72.3 antibody is directed to the detection of the STn antigen, the tumor-associated truncated glycan [18,21] expressed in MKN45 SC cell line, and absent in the control MKN45 WT cell line [37]. A NP functionalized with an unspecific IgG1 antibody was also developed to be used as a non-targeted control NP, NIgG. Our results showed that the main difference between functionalized and non-functionalized NPs is the PdI (Table 1). Besides the values being lower than 0.2, the functionalized NPs have higher values of PdI, showing that these NPs are more heterogenous and not so well distributed. This difference might be due to aggregation of NPs which may result from sample processing, during the functionalization protocol, using the carbodiimide process [42]. Nevertheless, by being vortex the NPs were resuspended again. In order to confirm the efficacy of NPs functionalization and quantify the conjugation efficiency (CE), an ELISA assay was performed. This indirect CE quantification was performed using the washes from functionalization method to quantify the antibody that did not bind. It was shown the presence of antibodies with CE of about 75% for IgG1 (from 33 μg) and around 85% in the case of B72.3 (from 33 μg), representing successful functionalization of NPs with both antibodies (Table 1). Previous studies report that low CE might be associated with lower amounts of antibody [34,43,44]. The high CE percentage observed in the developed NPs can be explained by the use of a high amount of antibody to functionalize these NPs, increasing the linkages between antibody and the NPs. To further confirm the CE, an ImmunoTEM characterization was performed showing the efficient binding of the antibody B72.3 to the nanoparticle as indicated by the black dot in the micrograph (Fig. 1E).

3.2. Characterization of lapatinib-loaded nanoparticles

The capacity of these NPs to encapsulate a Tyrosine Kinase Inhibitor (TKI) molecule with success was also evaluated and characterized. During the last two decades, several molecules targeting Receptor Tyrosine kinases (RTKs) were used as therapy in different types of cancer. TKIs are known as inhibitory drugs that can block the growth and spread of tumor cells by interfering with key molecules (RTK) involved in malignancy [45,46]. However, their effectiveness is limited by the acquired resistance or adverse effects like toxicity/side effects. These adverse effects can be avoided by TKI encapsulation in a nanosystem and deliver in a controlled manner [47–49]. Regarding Lapatinib, a dual tyrosine kinase inhibitor (HER2 and EGFR [24]), its clinically use is done in a restrictive form and is characterized by extensive albumin binding capacity, poor oral bioavailability, and poor water solubility, which results in poor and incomplete absorption from the gastrointestinal tract. Lapatinib is commercialized for oral intake only [50,51]. Therefore, it becomes imperative to formulate alternate efficient nano-delivery systems for administration through non-oral routes, for active targeting, and to scale-up by pharmaceutical scientists followed by their clinical trials by clinical experts. To overcome this obstacle, we developed a stable and high-loaded polymeric formulation encapsulating Lapatinib with the surface functionalized with mAbs against STn antigen. The physicochemical characterization can be assessed on Table A.1, as the association efficacy, drug loading and CE. The CE of antibodies was calculated by LC-MS and was made by a direct method of quantification, as we used the sample of NPs and after degraded enzymatically the antibody we proceeded to the analysis. The values of CE for B72.3 and IgG are ~65% (from 33 μg) for each. The values showed to be lower comparing to empty NPs, but we hypothesized that this can be due to the fact that the drug could limit the places to bind the antibody. Further, we also demonstrated the successful encapsulation, with an association of efficacy up to 50% of 1 mg of Lapatinib and a drug loading capacity of about 2.2%, quantified by a sensitive methodology, LC-MS, resulting in 20,467 mg of Lapatinib-loaded PLGA-PEG-COOH NPs per batch. On the literature, there are some reports that show higher levels for the percentage of encapsulation of Lapatinib. For example, Buss et al., reports an

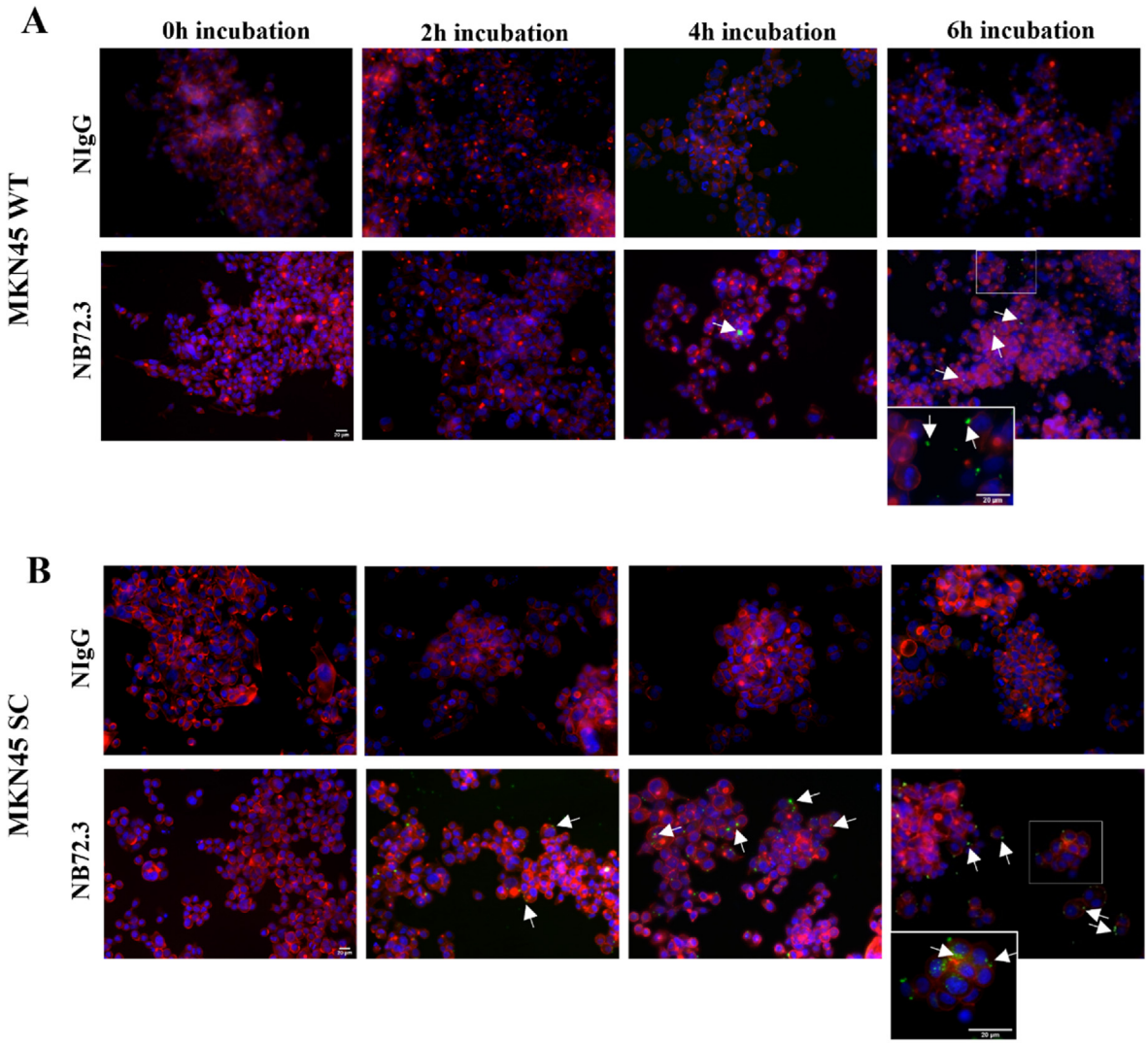

Fig. 3. Immunofluorescent staining of a panel of gastric cancer cells (MKN45 WT (A) and MKN45 SC (B)) incubated with NIgG and NB72.3 nanoparticles during different timepoints at 37 °C to evaluate the interaction between cell-nanoparticles under static fluid conditions. Nuclei are stained in blue, cytoskeleton (phalloidin) is stained in red and the antibody conjugated with the NPs are observed in green, the white arrow indicates the nanoparticles agglomerates. Images were acquired with magnification 20× for all timepoints and with magnification 63× for timepoint 6h. Scale bar: 20 μm.

association efficacy of 100% with a theoretical mass of 0.250 mg [52]. Taking this into consideration we can conclude that in our NPs we were able to encapsulate higher amounts of drug, 0.467 mg of Lapatinib. Lastly, we looked at the morphology of the NPs by ImmunoTEM which showed the presence of B72.3 on NP surface and the spherical shape of the NPs, indicating that these developed NPs are a good model to be applied in the future for drug delivery studies (Figure A.1).

Further, we performed a functional assay *in vitro* to evaluate the effect of the drug on the cancer cells with HER2 and EGFR amplification. We have used resazurin viability assay in GC cells expressing Sialyl-Tn (MKN45 SC) upon incubation with 1 μg/mL of Lapatinib, NLIgG and NLB72.3 during 24h and 48h. Our results showed that NLB72.3 induces higher specific effect, decreasing the metabolic activity in GC cells expressing STn at 24h and 48h of incubation (Figure A.2). Regarding the effect of NLIgG, this may stem from NPs sedimentation at static conditions and consequent unspecific release of Lapatinib.

3.3. *Interaction of gastric cancer cells and nanoparticles under static fluidic conditions*

In order to evaluate the capacity of the NPs functionalized with the antibody against the STn glycan to target tumor cells of interest we evaluated the interaction between gastric cancer cells with NPs under static fluid conditions followed by detection through flow cytometry. Empty B72.3 Functionalized PLGA-PEG NPs (NB72.3) and IgG Functionalized PLGA-PEG NPs (NIgG) (100 μg/ml) were incubated with MKN45 SC cells expressing STn and MKN45 WT cell line without expression of STn antigen. As seen in Fig. 2A, cell association was absent for non-targeted control, the NIgG, in both cell lines. On the contrary, a clear cell association was observed for NB72.3 with the STn expressing cell MKN45 SC, whereas no interaction was observed with MKN45 WT (Fig. 2B). The higher association and uptake of NB72.3 to MKN45 SC comparing to NIgG, shows the efficient target ability and specificity of these NPs. In other hand, the lack cell association was observed between NIgG and both cell lines, supporting that the NP recognition observed is specific (Fig. 2A). In fact, previous studies have shown that NPs targeting glycosylation have the potential to increase the specificity and therefore the safety and efficacy of carried therapeutic antitumor agents delivery [7,12]. Our results confirmed the capacity of recognition and specificity of the developed NPs targeting the cancer-associated STn glycan antigen. We also validated the capacity of recognition of our NPs in two other gastric cancer models: AGS WT and AGS SC (Figure A.3.A-B), without

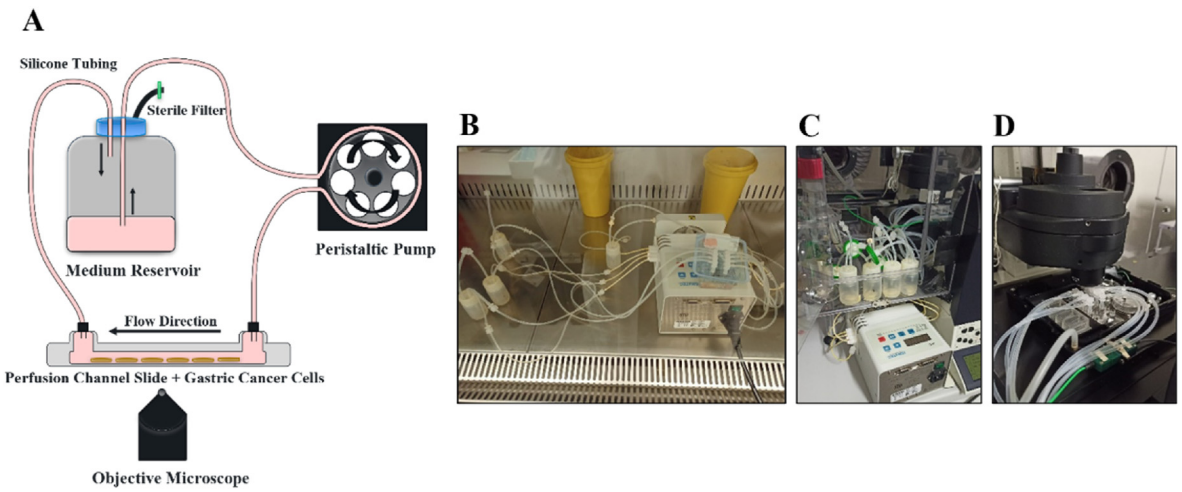

Scheme 2. (A) Schematic representation of methodology behind the development of studies under flow. (B) Mounting the microfluidic system in sterile conditions. (C) Widefield microscope with the peristaltic pump connected to the microfluidic system. (D) Perfusion channel slide connected by silicone tubing to microfluidic system and prepared to live acquisition by widefield microscope.

and with STn antigen expression, respectively. We demonstrated that NB72.3 and NIgG have a similar behavior with these two cell models comparing to MKN45 WT and MKN45 SC. We showed once more that they have efficient target ability and specificity.

Further evaluation of the specificity of the antibody covalently linked to the NP surface, was performed using a control experiment with B72.3 Adsorbed PLGA-PEG NPs (NAdsB72.3). We incubated B72.3 antibody with NPs in the absence of EDC and NHS and therefore without the activation of the carboxylic group to react to the amine group of the antibody. Nanoparticles NAdsB72.3 showed lower capacity of binding to cells expressing STn (MKN45 SC) (Fig. 2C) demonstrating that these NPs are not able to detect the STn expressing cells, and indeed requires the NP with the covalently linked antibody NB72.3. Overall, our data demonstrate the specificity of the conjugation method and highlights the importance of the NP displaying the covalently linked antibody. Our results are in agreement with a previous study with PLGA-NPs functionalized with aptamers in the presence and absence of EDC and NHS, that demonstrates the specificity of their conjugation reaction [53]. We also wanted to demonstrate that when we treat MKN45 SC with the neuraminidase enzyme to remove sialic acid groups, our NPs functionalized with antibody against STn antigen, are still showing specificity. Our results confirm the specificity of NB72.3 and the increase of Tn antigen upon treatment with neuraminidase enzyme, demonstrating that the treatment was efficient (Figure A.3. C).

To gain insight into the cellular and intracellular localization of the NPs, we examined the targeting ability and specificity of our polymeric NPs by immunofluorescence. The different cell models were incubated during different timepoints (0, 2, 4 and 6h) with functionalized NPs (100 μg/mL) in static fluid conditions (Fig. 3). Aggregates of NB72.3 were observed to have a much higher cell affinity to MKN45 SC, when comparing with the NIgG, which is practically undetectable the binding to MKN45 SC (Fig. 3B, arrow). In fact, NIgG behaved exactly as a non-targeted NP showing no binding to both cell models. Additionally, the association of NB72.3 to MKN45 SC showed to be time-dependent, as an increase in the binding of particles over time was observed. However, accumulation of aggregates of NB72.3 were also found close to the MKN45 WT cells, particularly at incubations of $\geq$ 4h (Fig. 3A, arrow). This observation may stem from the static fluid conditions experiments. Previous studies have reported that in static conditions, NPs tend to be accumulated and deposited closed to or on top of the monolayer cells [28,30]. Such static condition can promote the unspecific interaction between the cells and NPs. On the other hand, in both experiments, we cannot exclude a limitation of the carbodiimide chemistry method, where the lack of control over the antibody orientation into the NP surface poses a primary disadvantage of this method and should be taken into consideration. The coupling between groups and crosslinkers is not selective and controlled, so if the antibody does not have the binding sites available due to the orientation into the NP, this will reduce the targeting opportunity [54]. Moreover, assuming that the binding sites for detection by the secondary antibody- HRP are not available, the signal detected will not be significant, although this not exclude the presence of the antibody on the NPs surface [54,55].

3.4. *Interaction of gastric cancer cells and nanoparticles under flow fluidic conditions*

The major purpose behind developing NPs for drug delivery applications is the optimization of parameters that influence cell-NPs interactions. A common approach is to perform validation of NPs using *in vivo* animal experiments. Our results under static conditions highlighted some important issues related to the sedimentation of NPs, resulting in their heterogeneous dispersion with the target cells, and accumulation of toxic waste products [28,30,56]. Therefore, a mechanical stress methodology for evaluating NP risk management, dynamic under flow conditions, drug delivery and avoiding extensive animal validations is needed. We evaluated the effect of dynamic culture conditions in several conditions. By applying such studies in the absence of NPs we could adjust several variables, such as the medium supplementation, the shear stress, and allowed to define a proper coating condition to maintain cell culture and set light exposure to avoid phototoxicity during imaging. Such conditions were defined until no significant difference in morphology was found under static or dynamic conditions for both cells expressing or not our target of interest.

Furthermore, we also studied the effect of shear stress (2dyn/cm2), generated by fluid flow through the channels, on adhesion of NPs to MKN45 SC and MKN45 WT cells. To do so, cells were incubated with different empty NPs labelled with FITC groups, functionalized and non-functionalized (100 μg/mL), and live cell imaging was performed using over 5,5h (Scheme 2). We have used a theoretical mass of 5% PLGA-FITC and since the FITC conjugation is covalent, early release of the fluorophore from NPs is not expected. Our results showed that the targeting ability and specificity of the NPs is maintained under flow conditions as aggregates of B72.3 Functionalized PLGA-FITC-PEG NPs (NF–B72.3) binding only to the MKN45 SC cell model were observed (Fig. 4B, arrows; **Vid. A.1–6**). Although the control IgG Functionalized PLGA-FITC-PEG NPs (NF-IgG) did not bind to any cell model, we were able to see that

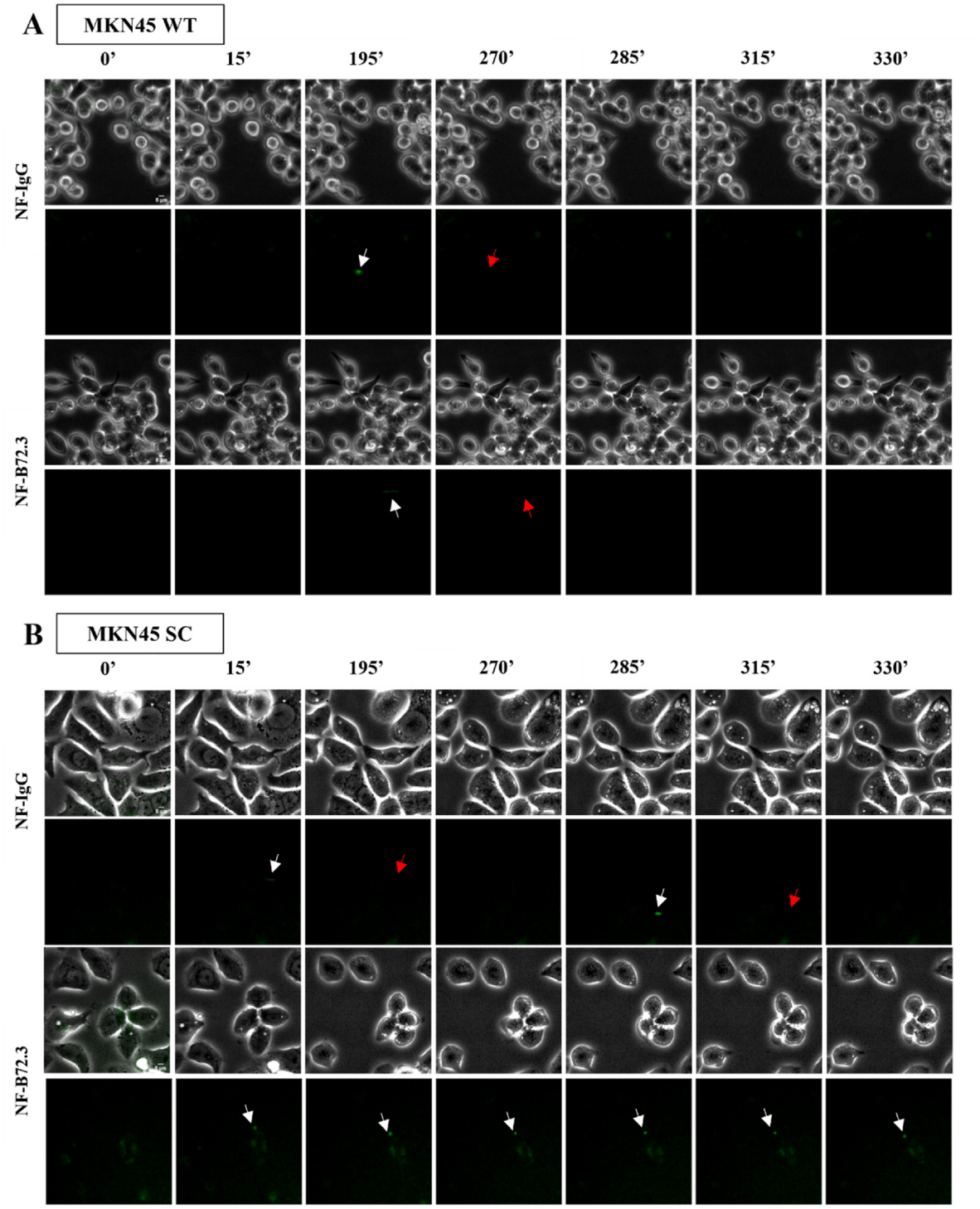

Fig. 4. Association of NFIgG and NFB72.3 to (A) MKN45 WT and (B) MKN45 SC after 5,5h incubation under live flow conditions (shear stress of 2dyn/cm2) at 37 °C. Representative images obtained with a widefield microscope at magnification 40×. Nanoparticles can be observed in green, the white arrow indicates the nanoparticles agglomerates, and the red arrow indicates when the nanoparticles disappear. The same brightness and contrast settings were used for the FITC (green) channel in all images. Scale bar: 5 μm.

both NPs labelled with FITC and functionalized appear to touch the cells in a non-specific way (Fig. 4, A-B, arrows; **Vid. A.1**–**6**). Nevertheless, the lack of adhesion of control NPs to cells further illustrates the specific targeting of this nanosystem to STn expressing cells. In contrast with the results observed under static conditions, we were able to avoid the unspecific accumulation of NPs aggregates under flow conditions, supporting the efficacy of this experiment for evaluation of the NPs interaction with the cells.

On the other hand, our results showed that cell morphology changes with several hours of live image acquisition exposure, suggesting a potential limitation of the current model of NP testing under flow conditions related to the maximum time of acquisition of images. These observations are most probably due to the shear stress, since the cells started to show signs of stress when following them over a very long period (more than 7h) (data not shown). Another reason that can support this observation, is the fact that contrarily to other studies, we performed

the live acquisition outside of an incubator. The proposed flow system is a novelty in the field as it allows to follow over time the interaction of NPs with the cells in live image acquisition. Most of the studies published so far rely on the fixation of the cells after a certain incubation period with the NPs under flow conditions, around 24h or 36h [26,27,32,57,58]. However, by doing so, we cannot infer about the interaction between them. In the future, this microfluidic system can be applied to the study of other nanoparticle–endothelial cell interactions, which can guide the engineering of NPs for *in vivo* medical applications. As example, shear stress-activated processes, in circulation, are reported to significantly affect the NP internalization by endothelial cells [26,27,57]. Therefore, several targeting strategies are employed to ensure the delivery of a sufficient payload of drug to the vascular regions under physiologic shear stress conditions, whereby the most promising experimental results have thus far been reported with endothelial adhesion molecule-targeting approaches [26,27,57,58].

Finally, we demonstrate that none of the compounds of the developed NPs (polymers or monoclonal antibodies) have a cytotoxic effect in our cell models during 5,5h and 24h, ensuring that our NPs do not affect the cell's metabolic activity (Figure A.4).

4. Conclusions

Our results showed that polymeric NPs functionalized with B72.3 antibody can target STn glycan, highly expressed by cancer cells. This is the first time that NPs functionalized with an anti-STn antibody were used for targeting STn expressing-cancer cells. Additionally, we evaluated the targeting capacity of these NPs in live cancer cells and under flow conditions. The live tracking of NPs is an innovative platform for *in vitro* experiments since it simulates the physiological flow which may mimics the behavior and interaction of cells and NPs in these conditions. Therefore, we propose that the live tracking using a microfluidic approach is a robust method to evaluate and characterize the targeting capacity the NPs and the effects they can have on the targeting cells. Finally, the specificity of these novel NPs demonstrates a great potential to be translated to *in vivo* studies of drug delivery.

Credit author statement

FD, JG, BS and CAR conceptualize the manuscript. FD and FS developed the nanoparticles and their functionalization. HO performed the mass spectrometry experiments. DC and FD developed the ELISA method. FD, MA and PS developed under flow experiments. FD prepared the schemes and figures. MA prepared the videos from under flow experiment. The manuscript was written through contributions of all authors. All authors have given approval to the final version of the manuscript.

Funding sources

This work was supported by the project Norte-01-0145-FEDER-000051 - "Cancer Research on Therapy Resistance: From Basic Mechanisms to Novel Targets", supported by Norte Portugal Regional Operational Programme (NORTE 2020), under the PORTUGAL 2020 Partnership Agreement, through the European Regional Development Fund (FEDER); and by National Funds through the Portuguese Foundation for Science and Technology (FCT): PTDC/MEC-ONC/0491/2021 and doctoral fellowship SFRH/BD/137896/2018 to FD.

Notes

The authors declare no competing financial interest.

Declaration of competing interest

The authors declare that they have no known competing financial interests or personal relationships that could have appeared to influence the work reported in this paper.

Acknowledgment

The authors acknowledge the support of the i3S Scientific Platforms: Advanced Light Microscopy and HEMS (Ana Rita Malheiro and Rui Fernandes), members of the national infrastructure PPBI - Portuguese Platform of Bioimaging (PPBI–POCI-01-0145-FEDER-022122); and Proteomics, member of the Portuguese Mass Spectrometry Network, integrated in the National Roadmap of Research Infrastructures of Strategic Relevance (ROTEIRO/0028/2013; LISBOA-01-0145-FEDER-022125).

Appendix A. Supplementary data

Supplementary data to this article can be found online at https://doi.org/10.1016/j.mtbio.2022.100417.

References

[1] H. Sung, et al., Global cancer statistics 2020: GLOBOCAN estimates of incidence and mortality worldwide for 36 cancers in 185 countries, CA A Cancer J. Clin. 71 (3) (2021) 209–249, https://doi.org/10.3322/caac.21660.
[2] E. Smyth, et al., Gastric cancer: ESMO Clinical Practice Guidelines for diagnosis, treatment and follow-up, Ann. Oncol. 27 (2016) v38–v49, https://doi.org/10.1093/annonc/mdw350.
[3] S. Raj, et al., Specific targeting cancer cells with nanoparticles and drug delivery in cancer therapy, in: Seminars in Cancer Biology, vol. 69, Elsevier, 2021, pp. 166–177, https://doi.org/10.1016/j.semcancer.2019.12.004.
[4] H. Khan, et al., Glyco-nanoparticles: new drug delivery systems in cancer therapy, in: Seminars in Cancer Biology, vol. 69, Elsevier, 2021, pp. 24–42, https://doi.org/10.1016/j.semcancer.2019.12.004.
[5] H. Yu, et al., Enzyme sensitive, surface engineered nanoparticles for enhanced delivery of camptothecin, J. Contr. Release 216 (2015) 111–120, https://doi.org/10.1016/j.jconrel.2015.08.021.
[6] S.-D. Li, L. Huang, Nanoparticles evading the reticuloendothelial system: role of the supported bilayer, Biochim. Biophys. Acta Biomembr. 1788 (10) (2009) 2259–2266, https://doi.org/10.1016/j.bbamem.2009.06.022.
[7] F. Diniz, et al., Glycans as targets for drug delivery in cancer, Cancers 14 (4) (2022) 911, https://doi.org/10.3390/cancers14040911.
[8] S. Acharya, S.K. Sahoo, PLGA nanoparticles containing various anticancer agents and tumour delivery by EPR effect, Adv. Drug Deliv. Rev. 63 (3) (2011) 170–183, https://doi.org/10.1016/j.addr.2010.10.008.
[9] S. Sharma, et al., PLGA-based nanoparticles: a new paradigm in biomedical applications, TrAC, Trends Anal. Chem. 80 (2016) 30–40, https://doi.org/10.1016/j.trac.2015.06.014.
[10] M.C. Operti, et al., PLGA-based nanomedicines manufacturing: technologies overview and challenges in industrial scale-up, Int. J. Pharm. 605 (2021), 120807, https://doi.org/10.1016/j.ijpharm.2021.120807.
[11] S. Rezvantalab, et al., PLGA-Based Nanoparticles in Cancer Treatment, Frontiers in pharmacology, 2018, p. 1260, https://doi.org/10.3389/fphar.2018.01260.
[12] S.A. Torres-Pérez, et al., Glycosylated nanoparticles for cancer-targeted drug delivery, Front. Oncol. (2020) 2667, https://doi.org/10.3389/fonc.2020.605037.
[13] S. Mereiter, et al., Glycosylation in the era of cancer-targeted therapy: where are we heading? Cancer Cell 36 (1) (2019) 6–16, https://doi.org/10.1016/j.ccell.2019.06.006.
[14] C. Gomes, et al., Expression of ST3GAL4 leads to SLex expression and induces c-Met activation and an invasive phenotype in gastric carcinoma cells, PLoS One 8 (6) (2013), e66737, https://doi.org/10.1371/journal.pone.0066737.
[15] S. Pinho, et al., Biological significance of cancer-associated sialyl-Tn antigen: modulation of malignant phenotype in gastric carcinoma cells, Cancer Lett. 249 (2) (2007) 157–170, https://doi.org/10.1016/j.canlet.2006.08.010.
[16] R. Soares, A. Marinho, F. Schmitt, Expression of sialyl-Tn in breast cancer correlation with prognostic parameters, Pathol. Res. Pract. 192 (12) (1996) 1181–1186, https://doi.org/10.1016/S0344-0338(96)80148-8.
[17] M. Inoue, et al., Expression of Tn and sialyl-Tn antigens in tumor tissues of the ovary, Am. J. Clin. Pathol. 96 (6) (1991) 711–716, https://doi.org/10.1093/ajcp/96.6.711.
[18] N.T. Marcos, et al., ST6GalNAc-I controls expression of sialyl-Tn antigen in gastrointestinal tissues, Front. Biosci. (Elite Ed) 3 (4) (2011) 1443–1455, https://doi.org/10.2741/E345.

[19] J. Munkley, The role of sialyl-Tn in cancer, Int. J. Mol. Sci. 17 (3) (2016) 275, https://doi.org/10.3390/ijms17030275.
[20] L. David, et al., Simple mucin-type carbohydrate antigens (Tn, sialosyl-Tn and T) in gastric mucosa, carcinomas and metastases, APMIS Suppl. 27 (1992) 162–172, https://doi.org/10.1007/s004280000218.
[21] N.T. Marcos, et al., Role of the human ST6GalNAc-I and ST6GalNAc-II in the synthesis of the cancer-associated sialyl-Tn antigen, Cancer Res. 64 (19) (2004) 7050–7057, https://doi.org/10.1158/0008-5472.CAN-04-1921.
[22] T. Ju, et al., Human tumor antigens Tn and sialyl Tn arise from mutations in Cosmc, Cancer Res. 68 (6) (2008) 1636–1646, https://doi.org/10.1158/0008-5472.CAN-07-2345.
[23] S. Julien, P.A. Videira, P. Delannoy, Sialyl-tn in cancer:(how) did we miss the target? Biomolecules 2 (4) (2012) 435–466, https://doi.org/10.3390/biom2040435.
[24] D. Freitas, et al., O-glycans truncation modulates gastric cancer cell signaling and transcription leading to a more aggressive phenotype, EBioMedicine 40 (2019) 349–362, https://doi.org/10.1016/j.ebiom.2019.01.017.
[25] K. Gidwani, et al., Europium nanoparticle-based sialyl-tn monoclonal antibody discriminates epithelial ovarian Cancer–Associated CA125 from benign sources, J. Appl. Lab. Med. 4 (3) (2019) 299–310, https://doi.org/10.1373/jalm.2018.028266.
[26] S.P. Samuel, et al., Multifactorial determinants that govern nanoparticle uptake by human endothelial cells under flow, Int. J. Nanomed. 7 (2012) 2943, https://doi.org/10.2147/IJN.S30624.
[27] L. Martínez-Jothar, et al., Endothelial cell targeting by cRGD-functionalized polymeric nanoparticles under static and flow conditions, Nanomaterials 10 (7) (2020) 1353, https://doi.org/10.3390/nano10071353.
[28] C. Fede, et al., Evaluation of gold nanoparticles toxicity towards human endothelial cells under static and flow conditions, Microvasc. Res. 97 (2015) 147–155, https://doi.org/10.1016/j.mvr.2014.10.010.
[29] O.C. Farokhzad, et al., Microfluidic system for studying the interaction of nanoparticles and microparticles with cells, Anal. Chem. 77 (17) (2005) 5453–5459, https://doi.org/10.1021/ac050312q.
[30] S.K. Mahto, T.H. Yoon, S.W. Rhee, A new perspective on in vitro assessment method for evaluating quantum dot toxicity by using microfluidics technology, Biomicrofluidics 4 (3) (2010), 034111, https://doi.org/10.1063/1.3486610.
[31] C. Freese, et al., In vitro investigation of silica nanoparticle uptake into human endothelial cells under physiological cyclic stretch, Part. Fibre Toxicol. 11 (1) (2014) 1–12, https://doi.org/10.1186/s12989-014-0068-y.
[32] F. Sambale, et al., In vitro toxicological nanoparticle studies under flow exposure, J. Nanoparticle Res. 17 (7) (2015) 1–12, https://doi.org/10.1007/s11051-015-3106-2.
[33] A.R. Garizo, et al., p28-functionalized PLGA nanoparticles loaded with gefitinib reduce tumor burden and metastases formation on lung cancer, J. Contr. Release 337 (2021) 329–342, https://doi.org/10.1016/j.jconrel.2021.07.035.
[34] I. Pereira, et al., Carcinoembryonic antigen-targeted nanoparticles potentiate the delivery of anticancer drugs to colorectal cancer cells, Int. J. Pharm. 549 (1–2) (2018) 397–403, https://doi.org/10.1016/j.ijpharm.2018.08.016.
[35] D. Colcher, et al., A spectrum of monoclonal antibodies reactive with human mammary tumor cells, Proc. Natl. Acad. Sci. USA 78 (5) (1981) 3199–3203, https://doi.org/10.1073/pnas.78.5.3199.
[36] H. Osório, et al., Proteomics analysis of gastric cancer patients with diabetes mellitus, J. Clin. Med. 10 (3) (2021) 407, https://doi.org/10.3390/jcm10030407.
[37] D. Campos, et al., Glycoengineered cell models for the characterization of cancer O-glycoproteome: an innovative strategy for biomarker discovery, Expet Rev. Proteonomics 12 (4) (2015) 337–342, https://doi.org/10.1586/14789450.2015.1059758.
[38] M. Thurnher, et al., Use of O-glycosylation-defective human lymphoid cell lines and flow cytometry to delineate the specificity of Moluccella laevis lectin and monoclonal antibody 5F4 for the Tn antigen (GalNAcα1-O-Ser/Thr), Immunol. Lett. 36 (3) (1993) 239–243, https://doi.org/10.1038/nmeth.2019.
[39] J. Schindelin, et al., Fiji: an open-source platform for biological-image analysis, Nat. Methods 9 (7) (2012) 676–682, https://doi.org/10.1016/0165-2478(93)90095-J.
[40] V.J. Yao, et al., Ligand-targeted theranostic nanomedicines against cancer, J. Contr. Release 240 (2016) 267–286, https://doi.org/10.1016/j.jconrel.2016.01.002.
[41] J. Conde, et al., Revisiting 30 years of biofunctionalization and surface chemistry of inorganic nanoparticles for nanomedicine, Front. Chem. 2 (2014) 48, https://doi.org/10.3389/fchem.2014.00048.
[42] H. Shen, A.M. Jawaid, P.T. Snee, Poly (ethylene glycol) carbodiimide coupling reagents for the biological and chemical functionalization of water-soluble nanoparticles, ACS Nano 3 (4) (2009) 915–923, https://doi.org/10.1021/nn800870r.
[43] E. Fernandes, et al., Glycoengineered nanoparticles enhance the delivery of 5-fluoroucil and paclitaxel to gastric cancer cells of high metastatic potential, Int. J. Pharm. 570 (2019), 118646, https://doi.org/10.1016/j.ijpharm.2019.118646.
[44] O.C. Farokhzad, et al., Targeted nanoparticle-aptamer bioconjugates for cancer chemotherapy in vivo, Proc. Natl. Acad. Sci. USA 103 (16) (2006) 6315–6320, https://doi.org/10.1073/pnas.060175510.
[45] M. Scheffler, et al., Clinical pharmacokinetics of tyrosine kinase inhibitors, Clin. Pharmacokinet. 50 (6) (2011) 371–403, https://doi.org/10.2165/11587020-000000000-00000.
[46] A. Jannin, et al., Tyrosine kinase inhibitors and immune checkpoint inhibitors-induced thyroid disorders, Crit. Rev. Oncol.-Hematol. 141 (2019) 23–35, https://doi.org/10.1016/j.critrevonc.2019.05.015.
[47] J.-H. Kim, et al., Polymeric nanoparticles for protein kinase activity, Chem. Commun. (13) (2007) 1346–1348, https://doi.org/10.1039/B612773H.
[48] A. Kumari, S.K. Yadav, S.C. Yadav, Biodegradable polymeric nanoparticles based drug delivery systems, Colloids Surf. B Biointerfaces 75 (1) (2010) 1–18, https://doi.org/10.1016/j.colsurfb.2009.09.001.
[49] B. Foroughi-Nia, et al., Progresses in polymeric nanoparticles for delivery of tyrosine kinase inhibitors, Life Sci. 278 (2021), 119642, https://doi.org/10.1016/j.lfs.2021.119642.
[50] N. Budha, et al., Drug absorption interactions between oral targeted anticancer agents and PPIs: is pH-dependent solubility the Achilles heel of targeted therapy? Clin. Pharmacol. Therapeut. 92 (2) (2012) 203–213, https://doi.org/10.1038/clpt.2012.73.
[51] H.A. Burris, et al., A phase I and pharmacokinetic study of oral lapatinib administered once or twice daily in patients with solid malignancies, Clin. Cancer Res. 15 (21) (2009) 6702–6708, https://doi.org/10.1158/1078-0432.CCR-09-0369.
[52] J.H. Buss, et al., Lapatinib-loaded nanocapsules enhances antitumoral effect in human bladder cancer cell, Front. Oncol. 9 (2019) 203, https://doi.org/10.3389/fonc.2019.00203.
[53] O.C. Farokhzad, et al., Nanoparticle-aptamer bioconjugates: a new approach for targeting prostate cancer cells, Cancer Res. 64 (21) (2004) 7668–7672, https://doi.org/10.1158/0008-5472.CAN-04-2550.
[54] M. Shen, J.F. Rusling, C.K. Dixit, Site-selective orientated immobilization of antibodies and conjugates for immunodiagnostics development, Methods 116 (2017) 95–111, https://doi.org/10.1016/j.ymeth.2016.11.010.
[55] J. Yang, et al., Antibody conjugated magnetic PLGA nanoparticles for diagnosis and treatment of breast cancer, J. Mater. Chem. 17 (26) (2007) 2695–2699, https://doi.org/10.1039/B702538F.
[56] J. Kim, R.C. Hayward, Mimicking dynamic in vivo environments with stimuli-responsive materials for cell culture, Trends Biotechnol. 30 (8) (2012) 426–439, https://doi.org/10.1016/j.tibtech.2012.04.003.
[57] H. Klingberg, et al., The influence of flow, shear stress and adhesion molecule targeting on gold nanoparticle uptake in human endothelial cells, Nanoscale 7 (26) (2015) 11409–11419, https://doi.org/10.1039/C5NR01467K.
[58] C. Fede, et al., Influence of shear stress and size on viability of endothelial cells exposed to gold nanoparticles, J. Nanoparticle Res. 19 (9) (2017) 1–13, https://doi.org/10.1007/s11051-017-3993-5.